Energy-per-Bit Limits in Plasmonic Integrated Photodetectors

Pierre Wahl, Takuo Tanemura, *Member, IEEE*, Christof Debaes, *Member, IEEE*, Nathalie Vermeulen, *Member, IEEE*, Jürgen Van Erps, *Member, IEEE*, David A. B. Miller, *Fellow, IEEE*, and Hugo Thienpont, *Member, IEEE*

***Abstract*—The energy consumption per transmitted bit is becoming a crucial figure of merit for communication channels. In this paper, we study the design tradeoffs in photodetectors, utilizing the energy per bit as a benchmark. We propose a generic model for a photodetector that takes optical and electrical properties into account. Using our formalism, we show how the parasitic capacitance of photodetectors can drastically alter the parameter values that lead to the optimal design. Finally, we apply our theory to a practical case study for an integrated plasmonic photodetector, showing that energies per bit below 100 attojoules are feasible despite metallic losses and within noise limitations without the introduction of an optical cavity or voltage amplifying receiver circuits.**

***Index Terms*—Bit error rate, nanophotonics, optical losses, photodetectors.**

I. Introduction

DURING last decade, there has been a growing discrepancy between the increase in processing performance per chip and the improvement of memory access bandwidth and delay. At the same time, the power consumption of electrical interconnects has become the limiting factor in the overall system performance [1]. For longer distances, optical fibers have alleviated the electrical interconnect bottleneck and optical interconnects are now ubiquitous for wide and metropolitan area networks. Also, on shorter distances, such as for local area networks, optical interconnects are replacing copper cables while offering increased bandwidth and less power consumption [1]. For the even shorter distances, between chips and on chips, the area available for wiring and for extracting the generated heat is limited. Consequently, the interconnect density and interconnect power consumption constitute the principal performance bottlenecks [2]. Hence, as pointed out in [3], optical interconnects can only be a viable alternative to electrical interconnects if they consume significantly less energy per transmitted bit. Much research has been carried out in the area of low-power photodetectors that report different performance metrics such as active volume [4] or gain bandwidth [5], [6] or which introduce a new photodetector design with better performance than other designs [7]. While all those performance metrics are valid, little attention has been paid to using energy consumption per bit as a specific design goal in photodetectors. Since this is one of the two principal bottlenecks in interconnects, we will, in this paper, investigate the design tradeoffs in photodetectors that arise when we choose to optimize the energy per bit.

This paper is structured as follows: first we briefly introduce the calculation of the energy per bit in a photodetector and a generic model for a photodetector; second, the tradeoffs that arise in each optimization are illustrated both analytically and by example using the simulated properties of a plasmonic germanium photodetector. We choose germanium because it is a very promising material for photodetectors given its CMOS compatibility and its high absorption coefficient up to the band edge at 1550 nm [8]. Finally, we draw conclusions.

II. Energy Consumption in Photodetectors

Optical interconnects can be more energy efficient than their electrical counterparts because it is not necessary to electrically charge the entire interconnect wire (at least over the pulse length) to the switching voltage of the receiver. Instead, only the electrical capacitance of the optoelectronic components, such as the modulator and the photodetector, need to be charged up to the switching voltage [9]. For photodetectors, the received optical energy E_p needed per bit is given by [3]

$$E_p = \frac{C_t V_d \hbar\omega}{e\Gamma} \tag{1}$$

where C_t is the total capacitance of the detector (including parasitic and receiver front-end capacitance), V_d is the switching voltage swing needed on the front-end amplifier, $\hbar$ is Planck's constant, ω is the angular frequency of the optical beam, and e is the elementary electron charge. $\Gamma \leq 1$ is the external quantum efficiency—the fraction of the incident photons that are absorbed by the device to generate electron–hole pairs—a factor that encompasses many nonidealities that increase the energy consumed per bit. For a fixed switching voltage and frequency, it is clear from (1) that the energy per bit in a photodetector is minimized by minimizing the ratio C_t/Γ. The parameters that determine C_t and Γ depend on the specific detector design

Manuscript received May 31, 2012; revised September 17, 2012; accepted October 28, 2012. Date of publication November 15, 2012; date of current version April 3, 2013. This work was supported in part by the Belgian American Education Foundation, the Methusalem and Hercules Foundations, Interuniversitary Attraction Poles, FWO-Vlaanderen, and the Interconnect Focus Center, one of six research centers funded under the Focus Center Research Programy, a Semiconductor Research Corporation entity.

P. Wahl, N. Vermeulen, J. V. Erps, and H. Thienpont are with the Brussels Photonics Team, Department of Applied Physics and Photonics, TONA-FIRW, Vrije Universiteit Brussel, 1030 Brussels, Belgium (e-mail: pwahl@b-phot.org; nvermeul@b-phot.org; jverps@b-phot.org; hthienpo@b-phot.org).

T. Tanemura is with the Department of Electronic Engineering, University of Tokyo, Tokyo 153-8904, Japan (e-mail: tanemura@ee.t.u-tokyo.ac.jp).

C. Debaes is with Dacentec, 9080 Lochristi Belgium (e-mail: christof@dacentec.com).

D. A. B. Miller is at the Edward L. Ginzton Laboratory, Stanford University, Stanford, CA 94305 USA (e-mail: dabm@stanford.edu).

Color versions of one or more of the figures in this paper are available online at http://ieeexplore.ieee.org.

Digital Object Identifier 10.1109/JSTQE.2012.2227687

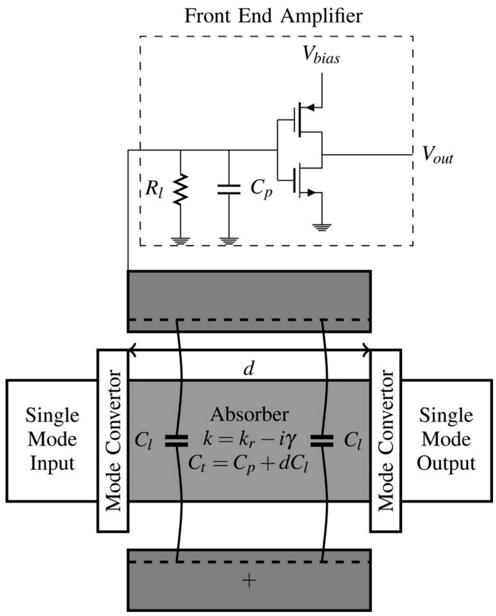

Fig. 1. Generic cavity-less photodetector. It features a single mode input and a perfect mode converter to the absorbing region. A perfect mode convertor couples the nonabsorbed light out of the detector, making it cavitiy less. The absorbing mode has an effective propagation constant k with an effective absorption constant γ. The total capacitance of the detector C_t depends linearly on the length of the detector with C_l as capacitance per unit of length plus a fixed parasitic capacitance C_p.

and include attributes such as material choice, size, electrical contacting and/or doping structure, and optical aspects such as front surface reflections, the choice of whether to use a resonator, and mode matching into resonators or waveguides. To study the main design tradeoffs, we propose a generic detector model that allows us to consider the influence of many of these design parameters on C_t/Γ, at least in the simplest useful approximations.

III. Generic Cavity-Less Photodetector Model

In this paper, we assume that all the light that reaches the photodetector is contained within a single optical mode. This framework includes waveguide-based photodetector designs [10], [11], where the light is coupled in through a single mode waveguide, as well as surface-normal designs [12], where the incoming mode can be approximated by a plane wave. In devices without a resonant cavity, detector operation is based on the absorption of light as it travels through an absorbing medium for a certain length. Given a particular lateral structure, this length determines the size of the detector. The longer this interaction distance is, the more light is absorbed in a single pass. To formalize this intuitive definition, we use a detector model as depicted in Fig. 1, where only one propagating optical mode with propagation constant $k = k_r - i\gamma$ is assumed in the absorbing region. This principle has often been implemented in waveguide-based devices [10], [13] and shows no optical bandwidth limitations beyond the material absorption bandwidth.

In addition to cavity-less photodetectors, a resonance could be used to enhance the interaction with the photoabsorber. The cavity can be formed by a ring resonator [14] or integrated waveguide resonators [15], [16] for waveguide-coupled devices. Being resonant, these devices always have some limit to their optical bandwidth, and will be somewhat harder to make because of the necessity of tuning the resonance to the desired operating wavelength. As will become clear in this paper, plasmonic photodetectors can be made very short without the introduction of a cavity. Therefore, we will restrict this paper to the simplest structures, considering only cavity-less devices.

We assume a mode coupler that couples the light from the incoming single mode source to the absorbing mode without reflections and independent of wavelength. After propagation over a distance d in the absorber, the remaining light of the optical mode is presumed to be perfectly coupled out without any back reflections. Though not all detectors will be so ideal, finite coupling losses could be added in later, at least as long as the detector is strongly enough absorbing that back reflections do not lead to resonances inside the detector. The fraction A of the optical power that is absorbed within the detector (either in the semiconductor or the metal) is, therefore, given by

$$A = (1 - e^{-2\gamma d}) < 1. \tag{2}$$

The generated photocarriers are collected by contacts placed parallel to the propagation direction of the optical mode that needs to be absorbed. The generated current is then amplified by a front-end amplifier to generate an isolated output voltage that will drive subsequent electrical stages. The contacts are assumed to have a capacitance *per unit of length* C_l while the front-end amplifier contributes to the parasitic capacitance C_p that is fixed and does not depend on the length of the detector. The total capacitance at the front end is given by $C_t = C_l d + C_p$. In fact, we assume that, when the size of the detector is increased, the total capacitance increases *linearly* with d while the nonabsorbed power decreases *exponentially* with the detector length. We believe that this trend holds in most nonresonator photodetector designs.

In photodetectors, only a fraction of the absorbed power leads to the creation of electron–hole pairs in the semiconductor. Some of the power is, for example, optically absorbed by metallic contacts if the optical field of the mode reaches them (as it may well do in plasmonic designs). To account for those losses, we define the semiconductor absorption fraction η_{abs} as the ratio of the useful power absorbed in the semiconductor to the total absorbed power. Calculating this ratio from first principles yields

$$\eta_{\mathrm{abs}} = \frac{\int_{\mathrm{SC}} \mathrm{Im}(\varepsilon_{\mathrm{SC}})|\mathbf{E}|^2 dS}{\int_{\mathrm{TOT}} \mathrm{Im}(\varepsilon)|\mathbf{E}|^2 dS} \tag{3}$$

where Im denotes the imaginary part of the relative permittivity, SC refers to the area covered by the semiconductor, and TOT refers to the entire mode area. Here, for simplicity, we neglect any absorption in the semiconductor regions that does not lead to photocurrent, such as free-carrier absorption, on the presumption that it will be weak compared to direct optical absorption in the semiconductor.

Assuming the best possible resulting external quantum efficiency ($\Gamma = \eta_{\mathrm{abs}} A$) and utilizing (1) we obtain the following equation for the energy per bit:

$$E_p = \frac{(C_l d + C_p) V_d \frac{\hbar\omega}{e}}{\eta_{\rm abs} A} = \frac{(C_l d + C_p) V_d \frac{\hbar\omega}{e}}{\eta_{\rm abs}(1 - e^{-2\gamma d})}. \tag{4}$$

We now calculate the length d_m that provides the minimum energy per bit, for a given C_l, C_p, γ, and $V_d \frac{\hbar\omega}{e}$, by the usual technique of finding where the derivative with respect to length becomes zero, i.e.,

$$\frac{\partial E_p}{\partial d}(d_m) = V_d \frac{\hbar\omega}{e} \frac{C_l - \frac{C_l + 2\gamma(C_p + C_l d_m)}{e^{2\gamma d_m}}}{\eta_{\rm abs}(1 - e^{-2\gamma d_m})^2} = 0. \tag{5}$$

To obtain an exact value of d_m, (5) needs to be solved numerically. To obtain insight, we distinguish the regimes in which the parasitic capacitance respectively dominates $(C_l \ll C_p\gamma)$ and does not dominate $(C_l > C_p\gamma)$. In the latter case, we obtain a solution for d_m that yields physical insight by making a third-order Taylor expansion of $\exp(2\gamma d)$ in the numerator of (5) and obtain

$$d_m \approx \sqrt{\frac{C_p}{C_l \gamma}} = \sqrt{L_c L_\gamma} \tag{6}$$

where $L_c = C_p/C_l$ and $L_\gamma = \frac{1}{\gamma}$. We note that the Taylor series converges for $C_l L_\gamma > C_p$. From (6), we observe that d_m equals the geometrical average of the *parasitic capacitance matching length* L_c that corresponds to the detector length needed to have the detector internal capacitance match the parasitic capacitance C_p, and the absorption length L_γ. This implies that a shorter optimal length is obtained by reducing the absorption length.

In addition, we note that as the parasitic capacitance tends to zero, the length of the most energy-efficient detector tends to zero ($d_m \to 0$), but the energy per bit $E_{\rm pm}$ still tends to a finite result equal to

$$E_{\rm pm} = \lim_{C_p \to 0} E_p = \frac{C_l V_d \frac{\hbar\omega}{e}}{2\eta_{\rm abs}\gamma}. \tag{7}$$

So, as the input capacitance of the front-end transistors is reduced as they are scaled down, it becomes increasingly beneficial to further reduce the size of the detector even *without enhancement of its sensitivity and despite the smaller number of photons absorbed*. It should therefore be stressed that, when the energy-per-bit figure of merit is applied, the design goal of absorbing nearly 100% of the incoming photons is not crucial. In addition, the *minimal achievable energy consumption per bit* for a given C_l, γ, and $\eta_{\rm abs}$ is given by (7), when $C_p = 0$.

In contrast, when the parasitic capacitance dominates $(C_l < C_p\gamma)$, the most energy-efficient solution is a long detector, absorbing almost 100% of the light. An accurate result for d_m can then only be obtained through an exact numerical solution of (5) and the optimal energy per bit can be approximated by

$$E_p = \frac{C_p V_d \frac{\hbar\omega}{e}}{\eta_{\rm abs}}. \tag{8}$$

It should be stressed that in this regime $\eta_{\rm abs}$ is the only optical property of the photodetector that has a nonnegligible influence on the energy per bit. For a given photodetector topology one could define the *equivalent parasitic capacitance* $C_{\rm pe}$

$$C_{\rm pe} = C_l L_\gamma. \tag{9}$$

When $C_p = C_{\rm pe}$ the contribution to the energy per bit of the parasitic capacitance E_1 [given by (10)] is equal to $E_2(d_m)$ [given by (11)], the contribution to the energy per bit of the detector capacitance with length d_m. E_1 and E_2 add up to the total energy per bit

$$E_1 = \frac{C_p V_d \frac{\hbar\omega}{e}}{\eta_{\rm abs} A} \tag{10}$$

$$E_2(d) = \frac{C_l d V_d \frac{\hbar\omega}{e}}{\eta_{\rm abs} A}. \tag{11}$$

It is, of course, important to minimize the parasitic capacitance overall, and good design here should make sure that the photodetector is integrated very close to the front-end transistors. Wiring will typically have a capacitance ∼100 s of attofarad per micrometer of length [3], so, when working with detector capacitances in the attofarad or low picofarad range, close integration (e.g., <100 nm − 1 μm) is very desirable; such close integration is, however, consistent with transistor and feature sizes in current and future silicon electronic technologies.

IV. Noise Limitations and Bit-Error Rate (BER)

So far, we have only focused on optimizing a generic photodetector so that a minimal energy per bit can load the input capacitance C_t to the switching voltage V_d. We have done this without taking into account the unavoidable intrinsic fundamental noise components in the photodetector that will limit the achievable BER. While the purpose of this paper remains to minimize the energy per bit we will, in this paragraph, illustrate how noise places a lower limit on the minimally required energy per bit for a given BER and electrical bandwidth, when using a photodetector that has been optimized using the technique described in the previous paragraphs. As detector noise cannot be analyzed without first considering the receiver circuit, we assume the use of a typical "receiverless" receiver architecture as depicted in Fig. 1. This receiver topology has a "high impedance" and should show excellent noise characteristics when the load resistance R_l is large (this topology could also be seen as a transimpedance amplifier with a very high feedback resistance, essentially eliminating the feedback). However, the large resistance R_l comes at the expense of the electrical bandwidth Δf_{RC} that depends on the total detector capacitance and the load resistance [17] and is defined as

$$\Delta f_{RC} = \frac{1}{2\pi R_l C_t}. \tag{12}$$

Without avalanching effects, the fundamental relation between the BER and noise is given by

$$Q = \frac{2RP_{\rm rec}}{\sqrt{\sum_i \sigma_{0i}^2} + \sqrt{\sum_i \sigma_{1i}^2}} \tag{13}$$

$$\mathrm{BER} = \frac{1}{2}\mathrm{Erfc}\left(\frac{Q}{\sqrt{2}}\right) \tag{14}$$

where $\sum_i \sigma_{0i}^2$ and $\sum_i \sigma_{1i}^2$ represent the total mean square of the current noise contributions when a "0" and a "1" are received, respectively [18]. $P_{\rm rec}$ in (13) is the required averaged input power to achieve a BER set by Q and under the noise figure set

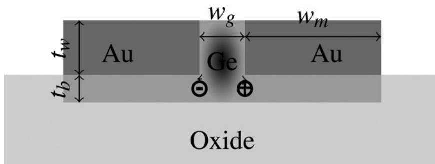

Fig. 2. Cross section of typical waveguide-based detectors. The waveguide mode is absorbed as it travels through the detector, creating electron–hole pairs that are extracted through the contacts.

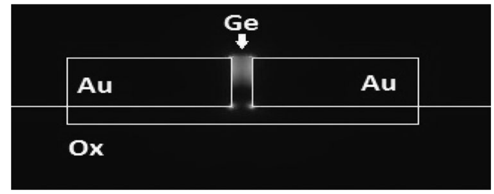

Fig. 3. Mode profile of a plasmonic waveguide mode.

by $\sum_i \sigma_{0i}^2$ and $\sum_i \sigma_{1i}^2$, R is the responsivity of the detector, and Q is linked to the BER through (14).

In order to calculate $\sum_i \sigma_{0i}^2$ and $\sum_i \sigma_{1i}^2$, we follow the formalism set by Krishnamoorthy and Miller [19] and consider thermal noise in R_l, the short channel excess noise in the field effect transistor (FET), and the shot noise contributions of the photocurrent, of the dark current and of the gate leakage current through the gate of the front-end transistor. 1/*f* noise was not included in this analysis as noise contributions from low-frequency components can be avoided by using ac coupling or by using encoding techniques that do not make use of low-frequency components [19]. This yields (15) for $\sum_i \sigma_{0i}^2$ and (16) for $\sum_i \sigma_{1i}^2$

$$\sum_i \sigma_{0i}^2 \approx \frac{4k_b F_n T I_2 \Delta f}{R_l} + 2eI_2\Delta f(I_d + I_l) + 4k_b T\Gamma_n \frac{(2\pi C_t)^2}{g_m} I_3 \Delta f^3 \tag{15}$$

$$\sum_i \sigma_{1i}^2 \approx \frac{4k_b F_n T I_2 \Delta f}{R_l} + 2eI_2\Delta f(I_d + I_l + 2RP_{\mathrm{rec}}) + 4k_b T\Gamma_n \frac{(2\pi C_t)^2}{g_m} I_3 \Delta f^3 \tag{16}$$

where, F_n is the amplifier noise factor, k_b is Boltzmann's constant, T is the absolute temperature, Δf is the noise bandwidth, I_d is the dark current, I_l is the leakage current through the gate, Γ_n is the short channel excess noise factor, g_m is the transconductance of the FET, and C_t is the total capacitance at the front end. I_2 and I_3 are Personick integrals that depend on the exact temporal shape of the signal as can be found in [19] and the references therein. Also both shot and thermal noise statistics are assumed to be Gaussian. Note that the only difference between $\sum_i \sigma_{0i}^2$ and $\sum_i \sigma_{1i}^2$ is $2eI_2\Delta f(2RP_{\mathrm{rec}})$, the photocurrent contribution to the shot noise term.

For a given BER and bandwidth we substitute (15) and (16) in (13) and solve for P_{rec} and obtain (17), shown at the bottom of the page, where E_{pn} is the noise limited minimum energy per bit.

We now choose the load resistance R_l so that the noise bandwidth Δf equals the *RC* bandwidth Δf_{RC} as given by (12) and we take $R = \eta_{\mathrm{abs}}(1 - e^{-2\gamma d})e/(\hbar\omega)$. After substituting in (17) we obtain (18), shown at the bottom of the page. It can be seen from the first two terms in (18) that the photocurrent shot noise and thermal noise components are independent of the bandwidth Δf and that the noise limited energy per bit E_{pn} diverges for $d = 0$ for a finite Q. If, for a certain topology, $E_p(d_m) < E_{\mathrm{pn}}(Q, \Delta f)$, then the minimum energy per bit for this topology is not sufficient to overcome the noise components we considered here to achieve a certain BER, but still this will be the most energy-efficient solution at a higher BER. Conversely, if $E_p(d_m) > E_{\mathrm{pn}}(Q, \Delta f)$ the topology as calculated previously provides the most energy-efficient way of achieving the required communication link under our assumptions. To get a sense of the order of magnitude of C_l, C_p, γ, E_{pm}, C_{pe}, and E_{pn} in practical systems, we now apply this reasoning to a germanium plasmonic waveguide-based photodetector.

V. Case Study

A cross section of the plasmonic waveguide photodetector topology is depicted in Fig. 2. The absorptive region is made of intrinsic germanium. The germanium material is connected with gold contacts that are used to sweep out the electron–hole pairs generated by the absorbed light. In this case study, we vary w_g the width of the waveguide and t_w the thickness of the waveguide. In all simulations, the thickness of the germanium contact layer t_b and the width of the contacts w_m are fixed at 50 and 400 nm, respectively. In addition, we presume a wavelength of 1300 nm; at this wavelength, Ge has a very strong absorption coefficient and SiGe quantum well modulators have also been postulated [20]. In such a structure, there is a metal–insulator–metal plasmonic mode with a very small mode volume (see Fig. 3) and it shows significant metallic propagation losses [15]. Because plasmonic modes, on one hand, offer some possible uses in optical interconnects [21] but on the other hand feature high metallic losses [22], we think that the energy per bit is a very interesting metric to evaluate their performance. Here, we use a vectorial eigenmode solver to calculate the complex propagation constant k and we solve the Poisson equation to calculate the capacitance

$$P_{\mathrm{rec}} = E_{\mathrm{pn}}\Delta f \approx \frac{Q}{R}\left(Qe\Delta f + \left[\frac{4k_b F_n T I_2 \Delta f}{R_l} + 2eI_2\Delta f(I_d + I_l) + 4k_b T\Gamma_n \frac{(2\pi C_t)^2}{g_m} I_3 \Delta f^3\right]^{1/2}\right) \tag{17}$$

$$E_{\mathrm{pn}} \approx \frac{Q\hbar\omega}{e\eta_{\mathrm{abs}}(1 - e^{-2\gamma d})}\left(Qe + \left[8\pi k_b T F_n C_t + \frac{2eI_2(I_d + I_l)}{\Delta f} + 4k_b T\Gamma_n \frac{(2\pi C_t)^2}{g_m} I_3 \Delta f\right]^{1/2}\right) \tag{18}$$

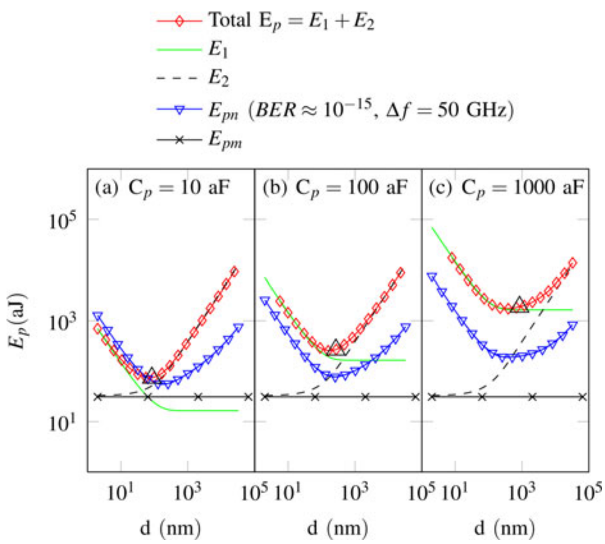

Fig. 4. Plots of the energy per bit and the noise limit $E_{\rm pn}$ as a function of the device length d. In each figure, the energy per bit is plotted for a specific parasitic capacitance (a) $C_p = 10$ aF, (b) 100 aF, and (c) 1000 aF and for $w_g = 50$ nm and $t_w = 50$ nm. Also, the black triangles denote the energy per bit for $d = d_m$ given by (6).

per unit length C_l between the contacts. The refractive indices at 1300 nm for gold $n_{\rm gold} = 0.4080 - 8.3028\ i$, germanium, $n_{\rm ge} = 4.3500 - 0.1i$, and oxide $n_{\rm ox} = 1.44$ were taken from [8]. For the calculation of C_l, the d.c. relative permittivities $\varepsilon_{\rm GeDC} = 16$ for germanium, and $\varepsilon_{\rm oxDC} = 2.07$ for silicon dioxide (the oxide in Fig. 2) were used. For gold's d.c. electrical conductivity (but not the optical or plasmonic propagation) we assume a highly conducting metal. Both simulations are performed using the finite-element-method-based tool COMSOL Multiphysics.

First we show the influence of the detector length d and the parasitic capacitance C_p on the energy per bit for a fixed photodetector topology with $w_g = t_w = 50$ nm. In Fig. 4(a)–(c), the energy per bit is plotted for different parasitic capacitances as a function of the detector length. The optimal detector length d_m given by (6) is denoted by a triangle in each plot. The contributions to the energy per bit of the parasitic capacitance E_1 and the detector capacitance E_2 are plotted separately. Their sum adds up to the total energy per bit. Also, the minimum achievable energy per bit $E_{\rm pm}$ is indicated by a cross (X). For calculating these energies, we presume that the switching voltage swing V_d needed on the front-end amplifier is 1 V. For a different required V_d, the energy will scale proportionally. Finally, the noise-limited minimum energy per bit $E_{\rm pn}$ is plotted assuming $Q = 8$, which sets the BER to 10^{-15}. The amplifier noise factor was set to $F_n = 3$ dB, the temperature was set to $T = 300$ K, and the bandwidth was chosen as $\Delta f = 50$ GHz. The dark current I_d was approximated as the dark current in a reverse biased metal semiconductor metal junction. For I_d, we used the regular expression for the current density across a Schottky barrier of height ϕ

$$I_d = t_w d_m R_d T^2 \exp(-e\phi/(k_b T)) \tag{19}$$

where $R_d = 120\ {\rm A/cm^2K^2}$ and where we took $\phi = 0.25$ eV [23]. Realistic dark currents for $t_w = w_m = 50$ nm are about 25 nA. For $I_l = j_l A_g$, we used a current density $j_l = 0.13^4\ {\rm A/m^2}$ as was found in the international technology roadmap for semiconductors (ITRS) road map for "low standby power logic" [24] and a corresponding gate surface $A_g = 22\ {\rm nm} \times 200$ nm. Low standby power transistors tend to have thicker gate oxide to reduce leakage that reduce the gate capacitance and the transconductance but increases the threshold voltage [24]. This increase is acceptable because of the chosen 1-V swing on the detector. For the Personick integrals, we chose $I_2 = 0.6$ and $I_3 = 0.09$ as is chosen in [19]. Finally, for the excess short channel noise, we estimated the transconductance $g_m = 140\ \mu S$ by using the linear model [25] and by using the maximum drain source current found in the ITRS road map for the 22-nm technology [24]. Also, we used an excess noise factor $\Gamma_n = 3$, which seems to be in the range of what has been presented in literature until gate lengths of 60 nm [26]. In our example, we found that the noise figure of our detectors was mainly dominated by the finite responsivity R for small detectors lengths d and by thermal noise that is about five times greater than other contributions in this example.

When C_p is 10 aF, which is extremely small, we can see from Fig. 4(a) that the contribution of the parasitic capacitance is almost negligible. The ideal detector length d_m is 90 nm, which is very close to zero, and the optimal energy per bit is roughly $E_{\rm pm}$ as given by (7). Here, we are clearly in the regime where $(C_l > C_p\gamma)$. Also we have $E_{\rm pn} = 70$ aJ, while $E_p(d_m) = 75$ aJ, so we remain above the noise limit as calculated under our assumptions. As C_p is increased to 100 aF, we observe from Fig. 4(b) that the parasitic contribution roughly equals the detector contribution at $d = d_m$ and that we are well above the noise limit. The equivalent parasitic capacitance is $C_{\rm pe} \approx 25$ aF for this detector topology. In addition, (6) provides an accurate approximation for d_m. As C_p is increased even further to 1000 aF in Fig. 4(c), the parasitic capacitance entirely dominates $(C_l \ll C_p\gamma)$ and the energy per bit is given by (8). Also the detector capacitance C_l and the absorption length L_γ then have a negligible influence on the energetic performance of the photodetector. The fact that we predict quite low energies even with such a relatively large V_d is important in itself, and we will discuss this point more later.

We now calculate the C_l, L_γ, $n_{\rm eff}$, $\eta_{\rm abs}$, $E_{\rm pm}$, and $C_{\rm pe}$ of the integrated plasmonic photodetector as we vary the width w_g and the thickness t_w.

From Fig. 5 we observe that the absorption length of the plasmonic photodetector can be extremely short. Regardless of the thickness, L_γ becomes as short as 50 nm when w_g =10 nm. For larger w_g, L_γ remains smaller than 200 nm. As can be seen in Fig. 6, $\eta_{\rm abs}$ remains above 40% even for very small t_w and w_g, because of the strong absorption coefficient of germanium.

In Fig. 7, the capacitance per unit of length C_l is depicted. As would be expected from the a parallel plate approximation, C_l is approximately proportional to t_w/w_g. A very low C_l can still be reached for small w_g, as long as the thickness t_w is reduced proportionally. The ability to reduce the thickness of the contacts to minute dimensions is a property of plasmonic photodetectors

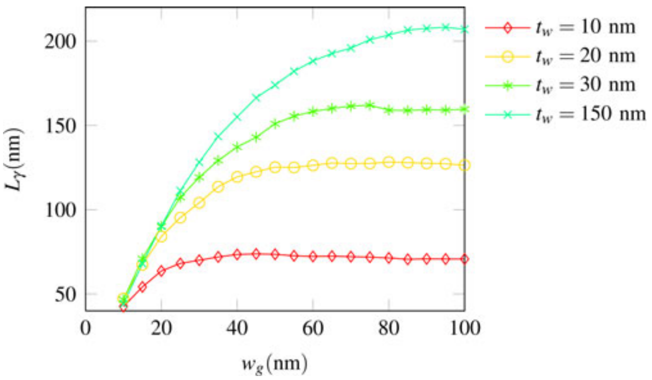

Fig. 5. Absorption length L_γ for different t_w as a function of w_g.

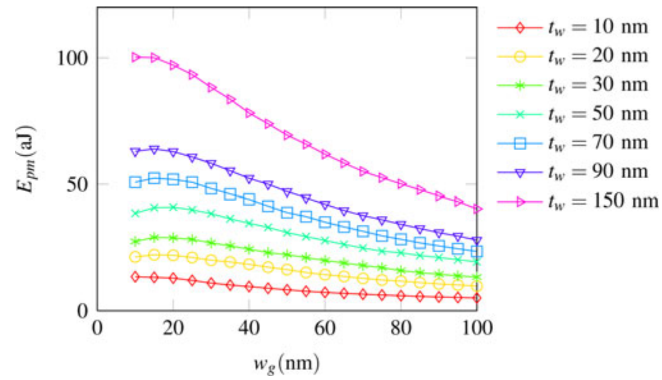

Fig. 8. Minimal energy per bit $E_{\rm pm}$ for different t_w as a function of w_g.

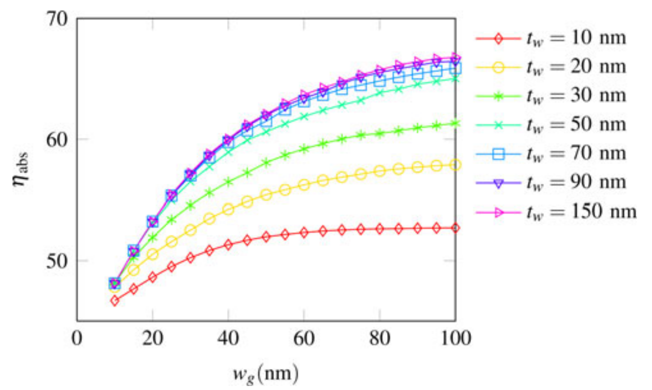

Fig. 6. Fraction of power of absorbed light $\eta_{\rm abs}$ in germanium for different t_w as a function of w_g.

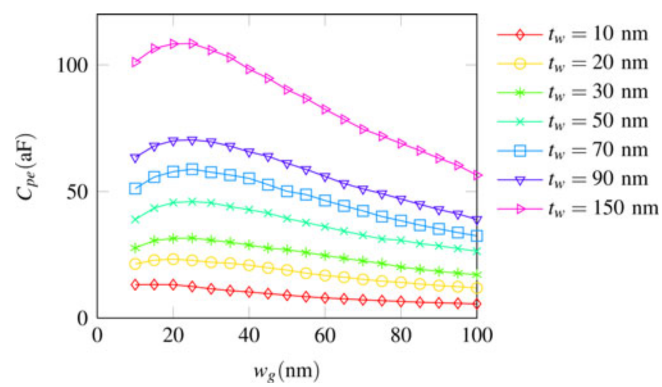

Fig. 9. Equivalent parasitic capacitance $C_{\rm pe}$ for different t_w as a function of w_g.

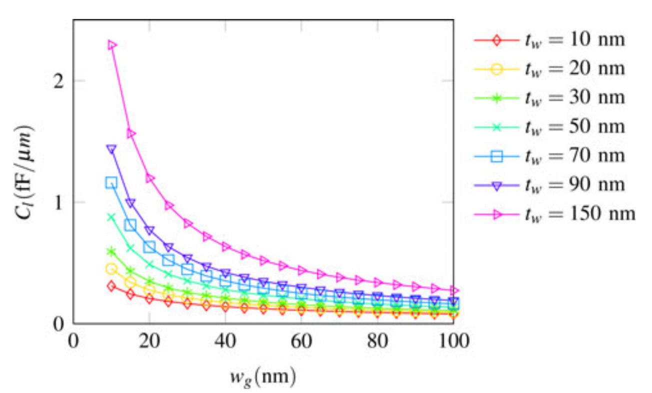

Fig. 7. Capacitance per unit of length C_l for different t_w as a function of w_g.

that cannot be replicated by a nonplasmonic equivalent; a nonplasmonic device at such small scales, would no longer be able to confine an optical mode substantially within the structure.

As shown in Fig. 8, a minimum achievable energy per bit $E_{\rm pm}$ between 10 and 100 aJ is reachable with this topology with V_d =1 V, despite the metallic losses. The lowest energy per bit is obtained when a very thin metal layer is used. However, to achieve this low level of energy per bit, the parasitic capacitance has to be reduced as well, below the equivalent parasitic capacitance $C_{\rm pe}$ depicted in Fig. 9, which lies between 20 and 100 aF. Currently, the best conventional front-end amplifiers still have an input capacitance well above this limit, for example, around $C_p = 30$ fF [27]. Lowering the parasitic capacitances of the front end to 10s to 100s of attofarads remains a necessary condition to make full use of the low-energy potential of a plasmonic photodetector. Otherwise, plasmonic photodetectors will likely remain less energy efficient than their nonplasmonic counterparts as the lower detector capacitance can no longer compensate for the metallic losses. The capacitance of the front-end amplifier can drop with downscaling of the transistors and by using more energy-efficient amplification schemes not based on the transimpedance amplifier [28], but the improvements needed are very substantial.

The basic design of such low-capacitance receiver circuits has been considered in principle before [19], [29], [30]. Traditional receiver circuits for telecommunications are often designed for the minimum received optical energy regardless of electrical power dissipation in the receiver circuit—not minimum total energy per bit—and are therefore designed to be limited by noise considerations. For conventional photodetectors with large capacitances, such noise optimization generally leads to wide input transistors with large g_m to minimize excess Johnson noise from the transistor channel [last term in (18)], which in turn leads to large receiver dissipation from the standing current in the transistor. Designing for minimum total energy per bit instead leads to much simpler receiver circuits; one optimum is to have a single CMOS transimpedance stage with near minimum-size transistors [19]. As previously mentioned, our very simple design that may be close to optimal in total energy

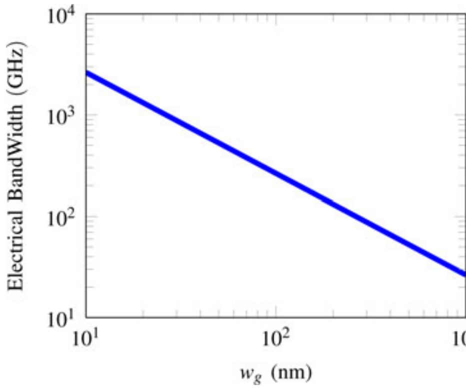

Fig. 10. Transit-time electrical bandwidth as a function of contact separation w_g.

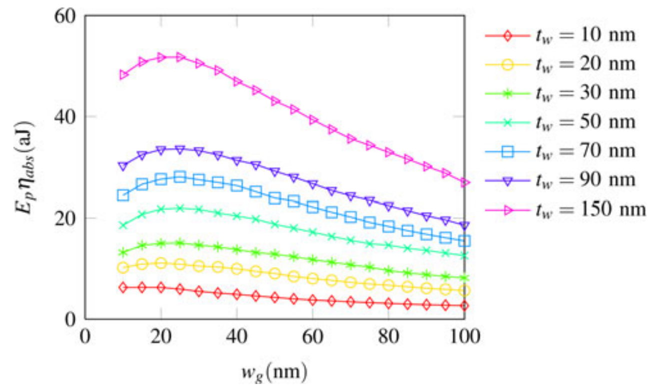

Fig. 11. Minimal energy per bit $E_{\mathrm{pm}}\,\eta_{\mathrm{abs}}$ neglecting metal losses for different t_w as a function of w_g.

is to eliminate voltage amplification altogether in the "receiverless" design; in such a design, the optically induced voltage change on the photodetector corresponds directly to the logic level swings needed in electronic logic circuits [19], [29], [30]. Our choice of V_d =1 V here is sufficiently large to run in this receiverless mode, in which case there is no electrical dissipation in voltage amplifiers and allowing for the use of high-threshold transistors with a thick gate oxide. Despite this large voltage swing, very low energy per bit within the noise limit is possible, as illustrated in our calculations, because of the use of very small, low capacitance detectors. With such approaches and with the continuing reduction in size and capacitance of future transistors, the necessary low parasitic capacitances that our detector approach here demands from the receiver circuit front end may be achievable.

VI. Energy per Bit and Electrical Bandwidth

The electrical bandwidth of a photodetector is limited both by the time it takes for the minority carriers to reach the contacts, referred to as the *transit-time bandwidth* [25], and by the *RC* constant of the electrical front end, referred to as the *RC bandwidth.* As the *RC-bandwidth* may be set by the electrical amplification scheme and by noise requirements, the *transit-time bandwidth* still is an upper limit on the achievable bandwidth, regardless of the amplification scheme used, and is found to be the limiting factor in many practical detectors [31]. The transit-time bandwidth f_t is proportional to the *saturated drift velocity* v_c in the semiconductor and inversely proportional to the width of the depleted semiconductor region (i.e., the distance between the contacts) [25]. Hence, f_t is given by

$$f_t = \frac{0.44\,v_c}{w_g}. \tag{20}$$

Using (20) and $v_{c\mathrm{Ge}} = 6.0 \times 10^4$ m/s [31], the transit-time electrical bandwidth of the plasmonic (and nonplasmonic) detector is plotted in Fig. 10 as a function of the waveguide width w_g. From Fig. 10, we can deduce that for an electrical bandwidth higher than 100 GHz a waveguide width smaller than 200 nm is required, and this is at the limit of what can be achieved with regular dielectric waveguides. Extremely high bandwidths of 1 THz are achievable for $w_g = 30$ nm that can be reached through plasmonics. (Though such bandwidths exceed those of current electronic amplifiers, such fast detectors could be used directly in applications such as photoconductive switches, e.g., for sampling for analog to digital conversion [32]).

From Fig. 8, we observe that for $w_g > 20$ nm the minimal achievable energy per bit increases as w_g is reduced. This can be attributed to an increasing C_l as w_g is reduced. In that regime, the electrical bandwidth comes at an energy cost per bit. However, for very narrow gaps $w_g < 20$ nm a smaller width w_g yields a slight reduction in minimal achievable energy per bit E_{pm}, despite the increase in C_l and lower η_{abs}. This is because the increase in C_l is compensated by the reduction of the absorption length L_γ, yielding more electrical bandwidth at a lower energy cost per bit, in spite of the increased metallic losses. This benefit may be partly due to an increase in the effective index of the mode at these small size scales, which in turn will lead to greater absorption in a given length of Ge. To show that, in our topology, the energy per bit is mainly determined by C_l/γ the minimal energy per bit with metal losses neglected $E_{\mathrm{pm}}\eta_{\mathrm{abs}}$ is plotted in Fig. 11. One can see that Fig. 11 is essentially only a scaled version of Fig. 8.

The fact that it is possible to achieve more bandwidth at lower cost per bit in our topology is merely a consequence of the fact the γ increases faster than C_l as w_g is lowered below 20 nm. In addition, we need to underline that the minimal energy per bit assumes a detector capacitance that is linearly dependent on the detector length and assumes no parasitic capacitance. As γ gets extremely large this assumption will break down as 3-D end effects will start to dominate the detector capacitance. These effects could be modeled as an intrinsic parasitic capacitance but the minimal energy per bit would rather be given by (8) than by (7). For our topology, solutions of the 3-D Poisson equation for a detector of finite length showed us that the detector capacitance is well approximated by the $C_l d$ until $d = t_w$ as can be seen in Fig. 12.

The relation between the energy per bit and the electrical bandwidth is illustrated in Fig. 13, where the minimal energy per bit E_{pm} of the analyzed plasmonic germanium photodetector is plotted for each electrical bandwidth f_t as calculated from (20). At lower bandwidths and large widths w_g, there is a tradeoff

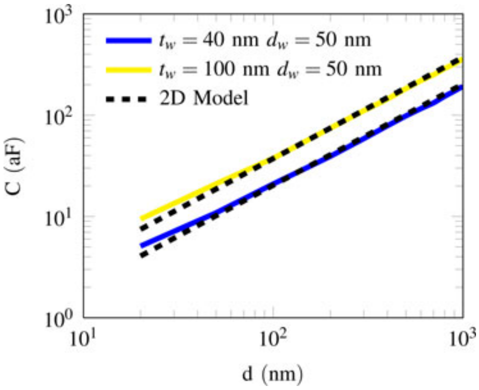

Fig. 12. Total capacitance of the full length detectors. The colored lines represent the full 3-D simulation, whereas the black dotted lines represent the 2-D model approximation.

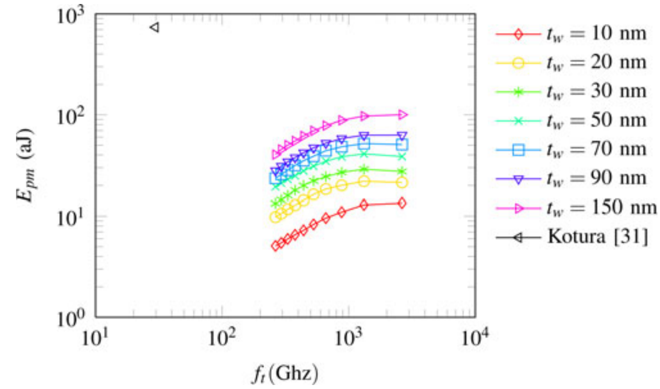

Fig. 13. Electrical bandwidth versus the minimum possible energy per bit $E_{\rm pm}$ for the plasmonic photodetectors and the Ge photodetector as published in [31].

between speed and energy per bit. At higher bandwidths and narrow widths this tradeoff no longer exists as narrower devices yield a lower energy per bit due to the dramatic reduction in absorption length. For the sake of comparison, we performed the same analysis for a nonplasmonic integrated germanium photodetector described in [31], as it perfectly matches our formalism and uses germanium as a photoabsorber with high quantum efficiency. A minimal achievable energy per bit $E_{\rm pm}=$ 700 aJ was obtained, which is approximately two orders of magnitude higher than what could potentially be achieved with the plasmonic topology, despite the losses.

VII. Conclusion

When the energy-per-bit metric is applied to a cavity-less waveguide photodetector, where the total capacitance consists of the sum of a capacitance that varies linearly with the detector's length and a fixed parasitic capacitance, we draw the following conclusions. The value of the parasitic capacitance distinguishes two regimes. First, when the parasitic capacitance dominates, the energy per bit is proportional to $C_p/\eta_{\rm abs}$. This means that the semiconductor absorption fraction $\eta_{\rm abs}$ is the only optical property of the photodetector that has an influence on the energy per bit. In this regime, plasmonic photodetectors will remain less energy efficient than regular larger dielectric solutions because of their metallic losses. For a given topology the equivalent parasitic capacitance limits this regime. This limit lies between 10 and 100 aF for the plasmonic detector we analyzed here. As this is much lower than the input capacitance of today's front-end amplifiers, current technology is still well within this parasitic-dominated regime. In addition, to keep C_p at these levels, the front-end transistor would presumably have to be placed very near the photodetector as the parasitic capacitance of their interconnection could be large. Second, when the parasitic capacitance drops below the equivalent parasitic capacitance, the ideal detector length that optimizes the energy per bit is equal to the geometric average of the absorption length and parasitic capacitance matching length. This length tends to zero as the parasitic capacitance is made zero while the optimal energy per bit converges to a finite minimal achievable energy per bit for a given photodetector topology. This minimum is proportional to $C_l/(\eta_{\rm abs}\gamma)$. In plasmonic detectors, the lower absorption fraction $\eta_{\rm abs}$ can, therefore, still be compensated by a lower C_l and an increased absorption constant γ as long as the parasitic capacitance is negligible. We calculated that a minimal energy per bit $E_{\rm pm}$ between 10 and 100 aJ in germanium-based plasmonic photodetectors, which is much lower than the $E_{\rm pm}$ we estimated for the dielectric equivalent found in [31]. We also point out that the noise limited energy per bit $E_{\rm pn}$ for such photodetectors is on the order of 70 aJ/bit at 50 GHz for a BER of 10^{-15}. Furthermore, we emphasize that the goal of this paper is minimize the energy per bit without optimizing for bandwidth nor for BER. Detectors whose minimal energy per bit are below the noise limit may still function at that energy per bit but with a higher BER. The found energies per bit presume, conservatively, that we are inducing 1 V of swing in the photodetector with the absorbed light. Such low energies per bit would, however, require very small receiver circuits with correspondingly low input capacitance, though such receivers appear to be possible in principle using CMOS amplifiers or by operating "receiverless," i.e., without any receiver voltage amplification, as is possible with our presumed 1-V swing. The lowest $E_{\rm pm}$ are achieved when very thin metals are used. We emphasize that, while substantial efforts have been delivered to reduce the waveguide gap, significant gains in energy per bit can also be achieved by reducing the metal thickness.

Acknowledgment

The authors would like to thank D. Ly-Gagnon for his valuable comments.

References

[1] A. F. Benner, M. Ignatowski, J. A. Kash, D. M. Kuchta, and M. B. Ritter, "Exploitation of optical interconnects in future server architectures," *IBM J. Res. Dev.*, vol. 49, no. 4.5, pp. 755–775, 2005.

[2] D. A. B. Miller, "Rationale and challenges for optical interconnects to electronic chips," *Proc. IEEE*, vol. 88, no. 6, pp. 728–749, Jun. 2000.

[3] D. Miller. (2009, Jun.). Device requirements for optical interconnects to silicon chips. *Proc. IEEE* [Online]. *97(7)*, pp. 1166–1185.

[4] L. Tang, S. E. Kocabas, S. Latif, A. K. Okyay, D.-S. Ly-Gagnon, K. C. Saraswat, and D. A. B. Miller. (2008, Mar.). Nanometre-scale germanium photodetector enhanced by a near-infrared dipole antenna. *Nature Photon.* [Online]. *2(4)*, pp. 226–229.

[5] Y. Kang, H. D. Liu, M. Morse, M. J. Paniccia, M. Zadka, S. Litski, G. Sarid, A. Pauchard, Y. H. Kuo, H. W. Chen, W. S. Zaoui, J. E. Bowers, A. Beling, D. C. McIntosh, X. Zheng, and J. C. Campbell, "Monolithic germanium/silicon avalanche photodiodes with 340 GHz gain–bandwidth product," *Nature Photon.*, vol. 3, no. 1, pp. 59–63, 2008.
[6] S. Assefa, F. Xia, and Y. A. Vlasov, "Reinventing germanium avalanche photodetector for nanophotonic on-chip optical interconnects," *Nature*, vol. 464, no. 7285, pp. 80–84, 2010.
[7] F. F. Ren, K. W. Ang, J. Ye, M. Yu, G. Q. Lo, and D. L. Kwong, "Split bull's eye shaped aluminum antenna for plasmon-enhanced nanometer scale germanium photodetector," *Nano Lett.*, vol. 11, pp. 1289–1293, 2011.
[8] E. D. Palik and G. Ghosh, *Handbook of Optical Constants of Solids*. New York: Academic, 1998.
[9] D. A. B. Miller, "Optics for low-energy communication inside digital processors: Quantum detectors, sources, and modulators as efficient impedance converters," *Opt. Lett.*, vol. 14, no. 2, pp. 146–148, 1989.
[10] O. Fidaner, A. K. Okyay, J. E. Roth, R. K. Schaevitz, Y. H. Kuo, K. C. Saraswat, J. S. Harris, and D. A. B. Miller, "Ge–SiGe quantum-well waveguide photodetectors on silicon for the near-infrared," *IEEE Photon. Technol. Lett.*, vol. 19, no. 20, pp. 1631–1633, Oct. 2007.
[11] Z. Zheng, A. M. Weiner, J. H. Marsh, and M. M. Karkhanehchi. (1997, Apr.). Ultrafast optical thresholding based on two-photon absorption GaAs waveguide photodetectors. *IEEE Photon. Technol. Lett.*, [Online]. *9(4)*, pp. 493–495.
[12] J. B. Heroux, X. Yang, and W. I. Wang, "Gainnas resonant-cavity-enhanced photodetector operating at 1.3 μm," *Appl. Phys. Lett.*, vol. 75, p. 2716, 1999.
[13] D. Ahn, C. Hong, J. Liu, W. Giziewicz, M. Beals, L. C. Kimerling, J. Michel, J. Chen, and F. X. Kärtner, "High performance, waveguide integrated Ge photodetectors," *Opt. Express*, vol. 15, no. 7, pp. 3916–3921, 2007.
[14] R. Shafiiha, D. Zheng, S. Liao, P. Dong, H. Liang, N. N. Feng, B. J. Luff, D. Feng, G. Li, J. Cunningham, and Others, "Silicon waveguide coupled resonator infrared detector," in *Proc. Opt. Fiber Comm. Conf.*, 2010, pp. 1–3.
[15] D. S. Ly-Gagnon, S. E. Kocabas, and D. Miller, "Characteristic impedance model for plasmonic metal slot waveguides," *IEEE J. Sel. Topics Quantum Electron.*, vol. 14, no. 6, pp. 1473–1478, Nov./Dec. 2008.
[16] A. R. M. Zain, N. P. Johnson, M. Sorel, and R. M. De La Rue, "Ultra high quality factor one dimensional photonic crystal/photonic wire microcavities in silicon-on-insulator (SOI)," *Opt. Express*, vol. 16, no. 16, pp. 12084–12089, 2008.
[17] S. B. Alexander, *Optical Communication Receiver Design*. Bellingham, WA: SPIE, 1997.
[18] G. P. Agrawal, *Fiber-optic Communication Systems*. vol. 222, New York: Wiley, 2011.
[19] A. V. Krishnamoorthy and D. A. B. Miller, "Scaling optoelectronic-vlsi circuits into the 21st century: A technology roadmap," *IEEE J. Sel. Topics Quantum Electron.*, vol. 2, no. 1, pp. 55–76, Apr. 1996.
[20] R. Schaevitz, E. Edwards, J. Roth, E. Fei, Y. Rong, P. Wahl, T. Kamins, J. Harris, and D. Miller, "Simple electroabsorption calculator for designing 1310 nm and 1550 nm modulators using germanium quantum wells," *IEEE J. Quantum Electron.*, vol. 48, no. 2, pp. 187–197, Feb. 2012.
[21] D. S. Ly-Gagnon, K. C. Balram, J. S. White, P. Wahl, M. L. Brongersma, and D. A. B. Miller, "Routing and photodetection in subwavelength plasmonic slot waveguides," *Nanophotonics*, vol. 1, pp. 9–16, 2012.
[22] A. Boltasseva and H. A. Atwater, "Low-loss plasmonic metamaterials," *Science*, vol. 331, no. 6015, pp. 290–291, 2011.
[23] U. Mishra and J. Singh, *Semiconductor Device Physics and Design*. New York: Springer-Verlag, 2007.
[24] International Technology Roadmap for Semiconductors (ITRS), Workgroup on Process Integration, Devices, and Structures (PIDS). 2010. Available: http://www.itrs.net/Links/2010ITRS/Home2010.htm
[25] S. M. Sze and K. K. Ng, *Physics of Semiconductor Devices*. New York: Wiley-Blackwell, 2007.
[26] C. H. Chen, B. Hung, S. Y. Huang, J. S. Jan, V. Liang, and C. S. Yeh, "Thermal noise performance in recent cmos technologies," in *Proc. IEEE 9th Int. Conf. Solid-State Integr.-Circuit Technol.*, 2008, pp. 476–479.
[27] A. Palaniappan and S. Palermo, "Power efficiency comparisons of interchip optical interconnect architectures," *IEEE Trans. Circuits Syst. II: Expr. Briefs*, vol. 57, no. 5, pp. 343–347, May 2010.
[28] A. Emami-Neyestanak, D. Liu, G. Keeler, N. Helman, and M. Horowitz, "A 1.6 Gb/s, 3 mW CMOS receiver for optical communication," in *Proc. IEEE Symp. VLSI Circuits Digest Tech. Papers, 2002*, pp. 84–87.
[29] C. Debaes, D. Argawal, A. Bhatnagar, H. Thienpont, and D. A. B. Miller, "High-impedance high-frequency silicon detector response for precise receiverless optical clock injection," *Proc. SPIE*, vol. 4654, pp. 78–88, 2002.
[30] C. Debaes, A. Bhatnagar, D. Agarwal, R. Chen, G. A. Keeler, N. C. Helman, H. Thienpont, and D. A. B. Miller, "Receiver-less optical clock injection for clock distribution networks," *IEEE J. Sel. Topics Quantum Electron.*, vol. 9, no. 2, pp. 400–409, Mar./Apr. 2003.
[31] D. Feng, S. Liao, P. Dong, N. N. Feng, H. Liang, D. Zheng, C. C. Kung, J. Fong, R. Shafiiha, J. Cunningham, A. V. Krishnamoorthy, and M. Asghari, "High-speed Ge photodetector monolithically integrated with large cross-section silicon-on-insulator waveguide," *Appl. Phys. Lett.*, vol. 95, pp. 261105–261105-3, 2009.
[32] R. Urata, L. Y. Nathawad, R. Takahashi, K. Ma, D. A. B. Miller, B. A. Wooley, and J. S. Harris, "Photonic a/d conversion using low-temperature-grown GaAs MSM switches integrated with Si-CMOS," *J. Lightw. Technol.*, vol. 21, no. 12, pp. 3104–3115, 2003.

Pierre Wahl received the B.S. degree in electrical engineering and the Erasmus Mundus M.S. degree in photonics from Vrije Universiteit Brussel (VUB), Brussels, Belgium, in 2007 and 2010, respectively. He wrote the Master's thesis at Interuniversity Microelectronics Center, Leuven, Belgium, in 2010, on high-frequency electrical voltage-controlled oscillators. He is currently working toward the Ph.D. degree in electrical engineering from VUB at the Brussels Photonics Team on low energy optical interconnects.

He joined the Miller Group, Stanford University, Stanford, CA, as a Visiting Researcher from 2010 to July 2011. His current research interests include optical interconnects and advanced simulation and optimization methods in nanophotonics.

Mr. Wahl has been a member of the International Society for Optics and Photonics since 2010.

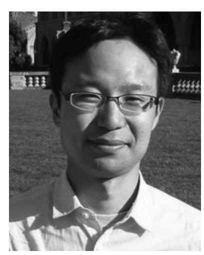

Takuo Tanemura (S'02–M'06) received the B.E., M.S., and Ph.D. degrees in electronic engineering, all from the University of Tokyo, Tokyo, Japan, in 2001, 2003, and 2006, respectively.

In 2006, he joined the Department of Electronic Engineering, the University of Tokyo and moved to the Research Center for Advanced Science and Technology, the University of Tokyo in 2007 as a Lecturer. In April 2012, he moved back to the Department of Electronic Engineering, the University of Tokyo, and became an Associate Professor. From March 2010 to February 2012, he was a Visiting Scholar at Ginzton Laboratory, Stanford University. His research interests include semiconductor photonic integrated circuits, nanophotonic and nanometallic devices, photonic switching networks, and optical interconnection.

Dr. Tanemura is a member of the Institute of Electronics, Information and Communication Engineers of Japan. He was the recipient of the 2005 IEEE Photonics Society Graduate Student Fellowships and Ericsson Young Scientist Award 2006.

Christof Debeas (S'99–M'04) was born in Geraardsbergen, Belgium, in 1975. He graduated with the academic degree of electrotechnical engineer from the Vrije Universiteit Brussel (VUB), Brussels, Belgium, in 1998, and the Ph.D. degree from the Applied Physics and Photonics Department in 2003, from VUB, in collaboration with the Ginzton Laboratory, Stanford University, Stanford, CA.

He is currently with Dacentec, 9080 Lochristi Belgium as Senior Engineer. He authored or coauthored more than 20 journal articles, more than 60 international conference proceedings, and two book chapters. His research interests include optical interconnects, Raman lasers, and the use of deep proton writing for the development of microoptical modules.

Dr. Debaes has been an Invited Speaker at three conferences. He was the recipient of Postdoctoraal Onderzoeker grant from the Research Foundation of Flanders. He is a member of the International Society for Optical Engineers, and IEEE Laser and Electrooptics Society.

Nathalie Vermeulen (S'06–M'08) was born in Duffel, Belgium, in 1981. She graduated with the academic degree of electrotechnical engineer with majors in photonics from the Vrije Universiteit Brussel (VUB), Brussels, Belgium, in 2004, and received the Ph.D. degree from the Applied Physics and Photonics Department, VUB, in 2008.

She is currently a Postdoctoral Researcher at the VUB. She has authored or coauthored 13 SCI-rated journal articles, and 24 international conference proceedings. Her research interests include the modeling of lasers, amplifiers, and converters based on Raman scattering and other nonlinear optical processes, and the development of mid-infrared laser sources.

Dr. Vermeulen has been an invited speaker at six conferences. She was the recipient of a Postdoctoraal Onderzoeker grant from the Research Foundation-Flanders. She recently also received the European Photonics21 Innovation Award. She is a member of the International Society for Optical Engineers, Optical Society of America, and IEEE Laser and Electrooptics Society.

Jürgen Van Erps (S'03–M'08) graduated as an Electrotechnical Engineer with majors in photonics at the Vrije Universiteit Brussel (VUB), Brussels, Belgium, in 2003 and received the Ph.D. degree from the same university in 2008.

In 2009 and 2010, he was a Visiting Researcher at the Centre for Ultrahigh bandwidth Devices for Optical Systems at the University of Sydney, Australia, under an Erasmus–Mundus Action 3 scholarship of the European Union. His research there involved high-resolution optical sampling of ultrahigh bitrate signals using dispersion-engineered highly nonlinear chalcogenide waveguides, and automatic dispersion monitoring and compensation of 1.28Tbaud links. He has authored or coauthored 26 SCI-stated papers and more than 75 papers in international conference proceedings. He is currently continuing his research at VUB on microcomponent prototyping, advanced field-installable fiber connectivity solutions, and mass deployable photonics-enhanced lab-on-a-chip devices for disruptive biosensing.

Dr. Erps won the BARCO/FWO High Tech Award for Scientific Research for the PhD thesis, entitled "Interfacing micro-components for optical interconnections from the FTTH-level to the PCB-level" in 2008. In 2003, he won theBARCO/FWO High Tech Award for Graduate dissertations and became a laureate of the K-VIV (Flemish Engineering Association) Prize for Engineers. He was the invited speaker at 17 international conferences. He is the co-inventor of one patent. He is a member of the Optical Society of America, and the IEEE Photonics Society, and a Senior Member of the SPIE.

David A. B. Miller (F'95) received the Ph.D. degree from Heriot-Watt University, Edinburgh, U.K., in physics in 1979.

He was with Bell Laboratories from 1981 to 1996, as a Department Head from 1987. He is currently the W. M. Keck Professor of Electrical Engineering, and a Co-Director of the Stanford Photonics Research Center at Stanford University, CA. His research interests include physics and devices in nanophotonics, nanometallics, and quantum-well optoelectronics, and fundamentals and applications of optics in information sensing, switching, and processing. He has published more than 250 scientific papers and the text *Quantum Mechanics for Scientists and Engineers*, and holds 69 patents.

Dr. Miller has been active in professional societies and was the President of the IEEE Lasers and Electro-Optics Society in 1995. He has received numerous awards, is a Fellow of Optical Society of America, American Physical Society, the Royal Society of London, and the Royal Society of Edinburgh, holds two honorary degrees, and is a Member of the US National Academy of Sciences and the US National Academy of Engineering.

Hugo Thienpont (M'99) was born in Ninove, Belgium, in 1961. He graduated with the academic degree of electrotechnical engineering in 1984 and received the Ph.D. degree in applied sciences in 1990, both from the Vrije Universiteit Brussel (VUB), Brussels, Belgium.

In 1994, he became a Professor at the Faculty of Applied Sciences, with teaching responsibilities in photonics. In 2000, he became the Research Director of the Department of Applied Physics and Photonics at the VUB, and in 2004, he was elected as the Chair of the Department. He is currently the Coordinator of several basic research and networking projects such as the European Access to Micro-Optics Expertise, Services and Technologies network. In addition to academic-oriented research projects, he manages microphotonics-related industrial projects with companies like Barco, Agfa-Gevaert, Tyco, and Umicore. He authored more than 220 SCI-stated journal papers and more than 400 publications in international conference proceedings. He edited 15 conference proceedings, authored seven chapters in books, and is the coinventor of 15 patents.

Prof. Thienpont was the Guest Editor of several special issues on *Optical Interconnects for Applied Optics* and the IEEE JOURNAL OF SELECTED TOPICS IN QUANTUM ELECTRONICS. He is the General Chair of the International Society for Optical Engineers Photonics Europe conferences in Strasbourg and Brussels. In 1999, he was the recipient of the International Commission for Optics Prize and the Ernst Abbe medal from Carl Zeiss. In 2003, he was awarded the title of IEEE Laser and Electrooptics Society Distinguished Lecturer. He was also the recipient of SPIE President's Award in 2005 for dedicated service to the European Community and the international Micro-Optics Conference Award in 2007. He was an Invited Speaker at 50 international conferences. He is a Fellow of the SPIE and EOS, and a member of the Optical Society of America, and the IEEE Photonics Society.